The Sensitivity of a Land Surface Parameterization Scheme to the Choice of Remotely Sensed Land-Cover Datasets

K. W. OLESON

Colorado Center for Astrodynamics Research, University of Colorado, Boulder, Colorado

K. L. DRIESE

Department of Botany, University of Wyoming, Laramie, Wyoming

J. A. MASLANIK AND W. J. EMERY

Colorado Center for Astrodynamics Research, University of Colorado, Boulder, Colorado

W. A. REINERS

Department of Botany, University of Wyoming, Laramie, Wyoming

(Manuscript received 2 April 1996, in final form 3 September 1996)

ABSTRACT

The characteristics of satellite-derived land-cover data for climate models vary depending on sensor properties and processing options. To better understand the first-order effects of differences in land-cover data on a land surface parameterization scheme (VBATS), stand-alone model runs were performed for two adjacent 2.8° × 2.8° GCM grid cells in Wyoming using land cover from two satellite-derived maps (AVHRR, TM) and a global land-cover dataset commonly used in GCMs.

The dominant cover type by area differed among the datasets for both grid cells. In the western grid cell, these differences resulted in substantially different surface fluxes simulated by VBATS. At spatial resolutions of 0.2° and 0.4°, the two satellite-derived datasets agreed on only 54%–62% of the land-cover types in both grid cells. Despite this disagreement, the VBATS simulated surface fluxes averaged over the grid cell were similar in the eastern grid cell for the two satellite-derived datasets. In the western grid cell, the partitioning of net radiation into sensible and latent heat fluxes was influenced by the dataset prescriptions of land-cover heterogeneity. In particular, the relative proportions of wet cover types (i.e., inland water and irrigated crop) had an effect on this partitioning, emphasizing the importance of accounting for the presence of wet cover types within a GCM grid cell in arid regions.

Spatial aggregation of the satellite-derived datasets reduced the number of land-cover types prescribed for each GCM grid cell. In the western grid cell, the reduction in the number of cover types from 11 to 2 resulted in differences in annual averages of sensible and latent heat fluxes of about 10%. Other simulations involving these datasets suggest that these differences could be reduced if one accounted for the wet cover types. In this respect, fine spatial resolution is required for some cover types, whereas coarser resolution may be adequate for other types. Land-cover classifications for land surface modeling need to be based more on model sensitivities than on traditional vegetation-type schemes.

1. Introduction

Due to computational constraints, general circulation models (GCMs) partition the earth's land surface into large grid cells (typically greater than 1° latitude by 1° longitude), with a single land-cover type assigned to each. These land-cover types provide a simple means for assigning to a grid cell a suite of distinct biophysical parameters that are used to estimate fluxes between the land surface and the atmosphere.

Land-cover datasets used within most GCMs are derived from a wide variety of map and atlas sources (e.g., Mathews 1983; Olson et al. 1983; Wilson and Henderson-Sellers 1985; Kuchler 1988). The accuracy of these datasets suffers from several limitations. Townshend et al. (1991) quantified the extent of these inadequacies by noting the significant disparities in estimates of cover-type area and spatial distribution between several ground-based datasets. Another significant drawback is that these maps cannot account for changes in land cover over time.

Corresponding author address: Keith W. Oleson, Colorado Center for Astrodynamics Research, University of Colorado, Boulder, CO 80309.
E-mail: oleson@frodo.colorado.edu

Remote sensing offers the most promising means for deriving improved global land-cover maps (Sellers et al. 1995; Townshend et al. 1991). Several issues arise, however, regarding choices in remote sensing instruments, classification methodology, and data processing to best meet the needs of GCMs (Hall et al. 1995). These issues are pertinent to remote sensing data processing and storage requirements during the Earth Observing System (EOS) era.

The Advanced Very High Resolution Radiometer (AVHRR) and the Thematic Mapper (TM) are two remote sensing instruments that have a long history as sources of land-cover information (Tucker et al. 1985; Townshend et al. 1987; Goward et al. 1985; Hopkins et al. 1988; Coleman et al. 1990; Saxena et al. 1992). To create land-cover datasets appropriate for climate modeling using these sensors, the choice of classification method should result in land-cover types that have distinct biophysical characteristics related to surface–atmosphere interactions. The interpretation of time series of spectral vegetation indices has recently become a common method for creating land-cover maps because of the relationship of these indices to vegetation characteristics (Loveland et al. 1991; DeFries and Townshend 1994; Townshend et al. 1994).

The resultant land-cover types must be ''mapped'' into the cover types defined by the land surface parameterization scheme (LSP). For example, Running et al. (1995) divide the world's land cover into six types. The ISLSCP Initiative I global land-cover dataset (Meeson et al. 1995) specifies 14 cover types. The Moderate Resolution Imaging Spectroradiometer (MODIS) Land Team proposes 19 cover types (three of which are nonvegetated land) for their MODIS Land Cover Product (Strahler et al. 1994). LSPs implemented in GCMs such as the Simple Biosphere Model (SiB) (Sellers et al. 1986) and the Biosphere–Atmosphere Transfer Scheme (BATS) (Dickinson et al. 1993) allow for 11 and 15 vegetated surface types, respectively. Consequently, the mapping rules used to translate the derived cover types into the appropriate LSP cover types warrant careful consideration. Mapping must not be based on simply matching cover-type labels but on the relevance of the cover type to the biophysical parameters specified within the LSP.

The spatial resolution of the remote sensing instrument is also an important consideration, especially with regard to the impact on data volume and aggregation methods. At AVHRR and TM spatial resolutions of 1.1 km and 30 m at nadir, respectively, both of these sensors are capable of providing land-cover data at resolutions that are much finer than can be used by current GCMs. However, these finer scales may be necessary for assessing the degree of land-cover heterogeneity and evaluating methods for scaling up to GCM grid-cell dimensions (Townshend et al. 1994). Fine spatial resolution land-cover information may also be required for other applications such as applying remote sensing algorithms to extract land-cover parameters (Hall et al. 1995) and to characterize land-cover transformations (Townshend and Justice 1988).

Land-cover data at AVHRR and TM spatial resolutions thus require some form of aggregation to match the coarser scales of the LSPs. Most GCMs specify a single land-cover type for each grid cell. The choice of land-cover type is typically resolved by selecting the dominant cover type present in the grid cell from the available land-cover maps (e.g., Dickinson et al. 1993). Evidence is mounting, however, that this homogeneous representation of land cover is unrealistic (Avissar 1992; Pielke et al. 1991; Henderson-Sellers and Pitman 1992). Thus, a variety of methods to account for land-cover heterogeneity within climate models have been proposed. Some researchers have applied statistics to important biophysical features that characterize the land surface. Both probability density functions (Entekhabi and Eagleson 1989; Avissar 1992; Boman et al. 1993; Collins and Avissar 1994) and simple averaging (blending) have been used (Henderson-Sellers and Pitman 1992; Verseghy et al. 1993). Alternatively, in the ''mosaic'' approach, land-cover types defined at subgrid spatial scales are regrouped into patches of homogeneous vegetation (Avissar and Pielke 1989; Koster and Suarez 1992). Surface fluxes are computed for each patch and area averaged to yield GCM grid-cell fluxes.

The goal of our work was to quantify the effects of some of the choices and information content inherent in remotely sensed land-cover datasets by incorporating these datasets at various spatial resolutions into the LSP component of a GCM. Specifically, we examined the effects of forcing a stand-alone vectorized version of the Biosphere–Atmosphere Transfer Scheme (VBATS) (Seth et al. 1994) with three land-cover datasets sampled at four spatial resolutions for two GCM grid cells in Wyoming. The influence of satellite-derived land-cover heterogeneity on simulated surface fluxes is investigated using the mosaic approach of Avissar and Pielke (1989). The two grid cells contain a broad range of land-cover types and thus offer a valuable test of the effects of mapping methods and scale.

Each dataset represents a different approach to land-cover mapping. The first, a standard map–atlas-based dataset (Olson et al. 1983 as adapted by Dickinson et al. 1993) is used in the National Center for Atmospheric Research (NCAR) Community Climate Model 2 (CCM2) GCM. The second is based on AVHRR data and was compiled at the EROS Data Center (EDC) using temporal normalized difference vegetation index (NDVI) profiles for the conterminous United States (Loveland et al. 1991). The third is based on photointerpretation of Landsat TM data at high resolution for the Wyoming domain and was constructed as part of the Gap Analysis Program (GAP) of the National Biological Service (Driese et al. 1996). We refer to these datasets as NC2, EDC, and GAP, respectively.

Through comparisons of output from VBATS simu-

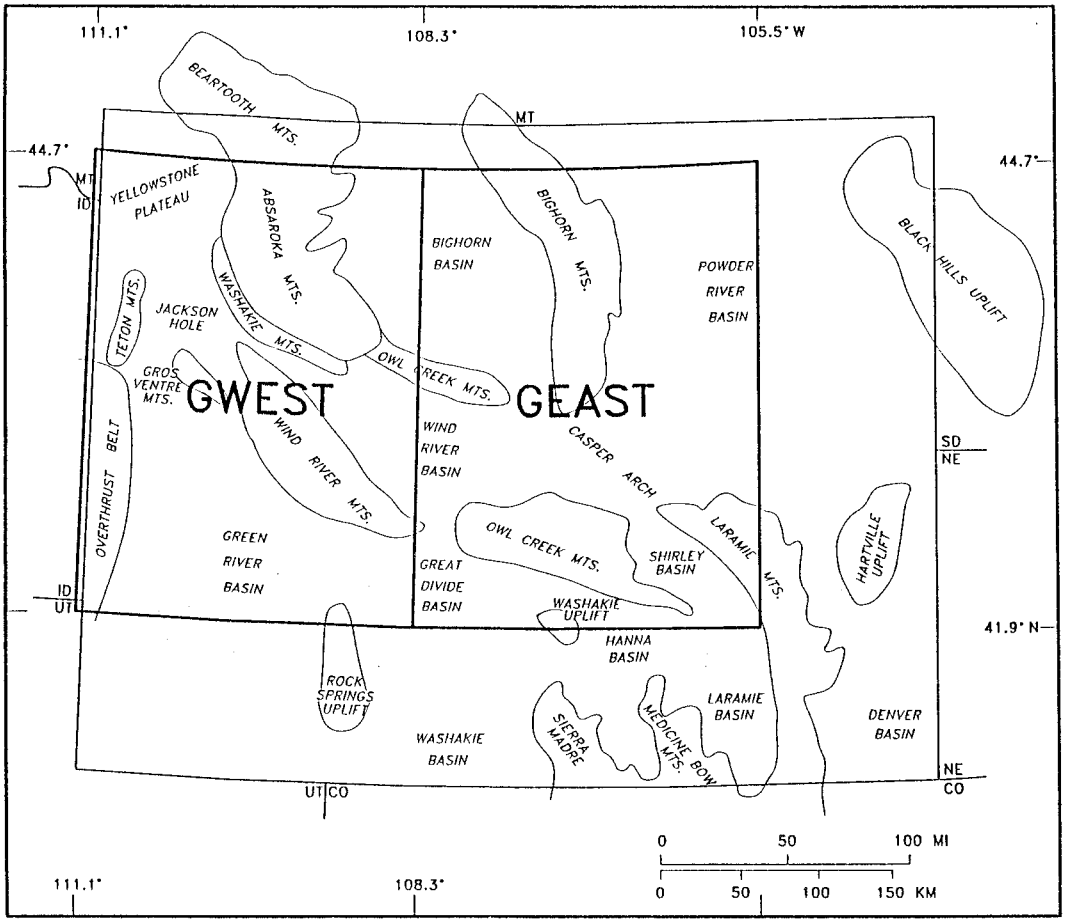

FIG. 1. The location of the two Wyoming GCM grid cells (denoted GWEST and GEAST) modeled. Both grid cells are 2.8° × 2.8° in size.

lations conducted with these datasets, this work addresses the following questions in the context of the two Wyoming GCM grid cells:

1) How does the land-cover composition of the two GCM grid cells differ as a function of the datasets and the degree of spatial resampling?
2) Is VBATS sensitive to differences in the dominant cover type prescribed by the three datasets?
3) Is VBATS sensitive to the differences in land cover prescribed by the EDC and GAP datasets at their finest spatial resolution?
4) Is VBATS sensitive to changes in prescribed land cover resulting from spatial aggregation of the datasets?

2. Approach

a. Study area description

The areas chosen for analysis correspond to two standard CCM2 2.8° latitude × 2.8° longitude grid cells contained within the state of Wyoming (Fig. 1). Both cells extend from 41.9° to 44.7°N. The western cell (denoted GWEST) extends from 108.3° to 111.1°W. The eastern cell (denoted GEAST) extends from 105.5° to 108.3°W. The two cells together include much of the variability in land cover typical of Wyoming and other parts of the intermountain west.

Most of Wyoming can be characterized as extensive basins separated by mountain ranges (Blackstone 1988) (Fig. 1). Elevations range from 939 to 4207 m above sea level with a mean elevation of 2030 m (Knight 1994). This high position coupled with a midcontinental location results in a generally cold, dry climate, although high relief between basins and mountain ranges causes wide variation in both precipitation and temperature. For most of the state, winters are cold and long. Summers are relatively short with temperatures above 32°C occurring on only a few days a year. Precipitation ranges from less than 15 cm to more than 150 cm per year in the mountains and averages 43 cm (Martner 1986).

The land cover of Wyoming varies with temperature, precipitation (amount and timing), soil, geology, dis-

turbance, and other environmental factors (Knight 1994). In general, the western portion of the state (and hence the GWEST grid cell) is dominated by mountain ranges. Evergreen and deciduous (mostly aspen) forest and herbaceous meadows in the mountains are interspersed with areas of primarily shrub-dominated basins. Eastern Wyoming (GEAST) is dominated by basins, but with some mountainous areas. The basins tend to be occupied by shrubs, although short-stature grasslands become more prevalent along the eastern one-third of the state.

b. Land-cover datasets

In addition to the contrasts offered by these land-cover types, the Wyoming domain was chosen as a test area due in part to the existence of land-cover data widely available to the modeling community (e.g., NC2 and EDC), along with the more highly refined and field-checked TM-based Wyoming Gap dataset (GAP). These three datasets represent different remote sensing platforms, spatial resolutions, land-cover mapping methods, and levels of field checking.

1) NC2

The NC2 dataset is equivalent to the NCAR CCM2 T-42 dataset described by Dickinson et al. (1993) and was derived by associating one of the 18 BATS types with each of the global vegetation types mapped by Olson et al. (1983). The Olson et al. dataset was originally constructed at $0.5^\circ \times 0.5^\circ$ resolution and included 46 land-cover types mapped globally from a variety of sources. The NC2 dataset was aggregated by assigning the dominant cover type (by area) to the GEAST and GWEST grid cells.

2) EDC

The U.S. Geological Survey EROS Data Center has developed a prototype land-cover characteristics database for the conterminous United States based on 1-km-resolution AVHRR NDVI data (Loveland et al. 1991; Brown et al. 1993). NDVI is calculated from the difference of near-infrared and visible surface reflectances normalized by their sum and has been correlated with modeling parameters such as annual net primary productivity (Goward et al. 1985), leaf area index (LAI) (Weiser et al. 1986), and fraction of photosynthetically active radiation (FPAR) (Sellers et al. 1992). Time series of the NDVI can assist in defining land-cover types based on their seasonal characteristics (Reed et al. 1994).

To create the EDC database, eight 4-week composites of maximum NDVI for the 1990 growing season (March to October) were clustered into 70 distinct spectral–temporal classes. These classes were subsequently divided into 159 classes based on ancillary data and phenological profiles.

To make this land-cover data more useful to the climate modeling community, the EDC has translated the 159 classes into land-cover types used by some LSPs (i.e., SiB and BATS). The EDC added 9 additional ''mixed'' classes to its BATS dataset to account for classes comprising a mixture of two or more of the 18 BATS classes. These mixed classes are incompatible with the BATS code as it currently exists. To resolve this problem, we used EDC descriptions of the composition of the mixed classes, including percent occupancy by the various mixture components, to translate the mixed classes into the 18 BATS classes. These assignments were usually based on the dominant BATS type (by area) in each mixed class. In certain areas, however, the combination of several nondominant land-cover types that were perceived to have similar biophysical parameters sometimes resulted in the second most dominant land-cover type being assigned to the pixel.

Inspection of the EDC BATS data revealed an additional problem in the mapping of western shrub types (A. Seth 1995, personal communication). Sparse shrublands in much of the Intermountain West and the Great Basin had been translated to the BATS evergreen shrub type by the EDC when in fact the parameters associated with the BATS semidesert type are more appropriate in most of these areas. To improve this assignment, annual NDVI profiles were generated from AVHRR data for each of the original EDC shrub classes occurring in the western United States. The original EDC western shrub classes were reassigned to the most appropriate BATS class, taking into account the fractional vegetation cover and LAI prescribed by BATS for each class. In some cases, existing vegetation maps were used to aid in the reclassification. The result is an improved EDC-based BATS landcover dataset for the United States.

3) GAP

The TM-based GAP dataset for Wyoming was assembled in response to the need for a highly resolved and accurate land-cover map of the state for use with animal habitat models in support of the National Biological Service Gap Analysis Program (Scott et al. 1993). Similar maps are in various stages of completion for other states. The GAP map is the finest-resolution land-cover map available for the state of Wyoming. It is based on extensive field reconnaissance and has been reviewed by land managers in Wyoming (e.g., the Bureau of Land Management and the U.S. Forest Service) (Driese et al. 1996). A formal statistical evaluation using airborne video is scheduled for 1997.

Construction of the Wyoming GAP land-cover map followed the methods of Davis et al. (1990) and is described in detail by Driese et al. (1995, unpublished manuscript). Degraded resolution (100 m) TM data were

used to create a digital false-color composite image that served as a basis for manual photointerpretation of nearly 17 000 vector polygons into 41 land-cover classes. The vector map was converted to a cell-based map and reclassified into the 18 BATS types based on the dominant BATS type in each of the original vector polygons. The reclassification was accomplished by assigning each GAP type to an appropriate BATS type before rasterization.

4) AGGREGATION

We aggregated the EDC and GAP datasets to coarser spatial resolutions to examine the effects of a coarser prescription of land cover on VBATS output. EDC and GAP datasets were resampled from their original resolutions to 0.2°, 0.4°, and 2.8° resolution cells by assigning the dominant BATS land-cover type (by area) from the finer-resolution data to each coarser-resolution cell.

c. Sensitivity of VBATS to the heterogeneous nature of land cover

1) MODEL DESCRIPTION

In the stand-alone version (i.e., uncoupled from the GCM atmosphere) of the VBATS model (Seth et al. 1994), the GCM grid cell is modeled as a higher-resolution grid of N^2 subcells. For example, the Wyoming 2.8° × 2.8° CCM2 grid cells were divided into subcell meshes consisting of $7^2 = 49$ and $14^2 = 196$ subcells of 0.4° × 0.4° and 0.2° × 0.2° size, respectively. A single land-cover type was assigned to each subcell. Each of the subcells has its own independent connection to the atmosphere, and horizontal interactions between subcells are not permitted. This approach allows for the modeling of land-cover heterogeneity while maintaining the relative location of each subcell within the GCM grid cell. This approach thus also allows for heterogeneity in atmospheric forcing, although we did not exploit this feature in our work.

To force the model with the land cover prescribed by the datasets at spatial resolutions of less than 2.8°, we adopted the mosiac approach to regroup subcells with identical land-cover types into a single subcell. The number of subcells for each simulation was therefore determined by the number of cover types in each version of the dataset. To yield GCM grid-cell fluxes, subcell fluxes were weighted according to each land-cover type's areal coverage within the 2.8° grid cell and then summed. This linear combination approach assumes that the atmosphere is well mixed within the surface layer and each subcell interacts independently within that surface layer. In reality, contrasts in the surface characteristics of adjacent land-cover types can act nonlinearly on surface fluxes under certain conditions (Pielke et al. 1991). For example, wind stress can be influenced in a nonlinear fashion by spatial patterns of roughness length. However, since these interactions are not currently modeled within GCMs, we have adopted the assumption of linearity as a first approximation for examining the influence of differences in satellite-derived land cover on surface fluxes.

The land-surface parameterizations within VBATS are identical to those of BATS (Dickinson et al. 1993), but the vectorized nature of the VBATS code allows for efficient simulations of multiple subcells. VBATS models the land surface using a single vegetation layer and a multiple-soil-layer scheme. Vegetation can be specified as one of 15 global types. To quantify the fundamental structural and physiological characteristics of each cover type, a set of biophysical parameters (e.g., vegetation fractional cover, roughness length, albedos for visible and near-infrared wavelengths, leaf area index) is specified by the model based on ecosystem field data. The seasonality of vegetation fractional cover and LAI is approximated through a dependence on the prognostic deep soil temperature ranging between maximum and minimum prescribed values.

Air temperature within the canopy and foliage temperature are calculated using an energy balance equation that includes canopy to ground, canopy to atmosphere radiative and sensible heat exchanges, transpiration, and evaporation of water/snow intercepted by the foliage. Transpiration is calculated from the aerodynamic resistance to moisture and heat flux of the foliage molecular boundary layer and a parameterization of stomatal resistance based on a set of environmental factors.

Sensible and latent heat and momentum fluxes are calculated using a standard drag coefficient parameterization. Drag coefficients, expressed as a neutral drag coefficient multiplied by a stability correction factor, are obtained for a grid cell by averaging coefficients over vegetation, soil, and snow-covered surfaces. The neutral drag coefficient is a logarithmic function of the lowest atmospheric model layer height and the roughness length of the surface. The stability correction factor is expressed in terms of the local Richardson number.

The soil is represented by two layers for temperature, a surface layer and a deep layer, and three layers for moisture. Soil temperature is solved for using modified equations of the force–restore method (Dickinson 1988). Soil moisture is predicted from water budget equations taking into account contributions from precipitation, leaf drip, evapotranspiration, groundwater and surface runoff, and the exchange of soil water between layers. Soil texture can be specified as one of 12 classes, ranging from sand to clay. The hydrologic characteristics of differing soil textures are governed by prescribed parameters of porosity, hydraulic conductivity, wilting point, etc., for each of the 12 classes. Soil albedos are specified by eight color classes, from light to dark, and as a function of the moisture content of the surface soil layer.

While a coupled atmosphere–surface model is needed

TABLE 1. Description of VBATS simulations. The first letter in the simulation name indicates west (W) grid cell or east (E) grid cell.

Simulation	Land-cover data source	Aggregation method	Number of subcells	Size of subcells	VBATS Land-cover type(s)
WEN, ESG	NC2	Dominant @ 2.8°	1	2.8° × 2.8°	Evergreen needle leaf (W), short grass (E)
WSD, ESD	EDC, GAP	Dominant @ 2.8°	1	2.8° × 2.8°	Semidesert (W, E)
WEDC.FR, EEDC.FR	EDC	Full resolution (1 km)	10(W), 9(E)	*	See Fig. 2a (W), Fig. 3a (E)
WGAP.FR, EGAP.FR	GAP	Full resolution (100 m)	11(W), 9(E)	*	See Fig. 2b (W), Fig. 3b (E)
WEDC.4, EEDC.4	EDC	Dominant @ 0.4°	7(W), 4(E)	*	See Fig. 2a (W), Fig. 3a (E)
WGAP.4, EGAP.4	GAP	Dominant @ 0.4°	2(W), 3(E)	*	See Fig. 2b (W), Fig. 3b (E)
WEDC.2, EEDC.2	EDC	Dominant @ 0.2°	8(W), 7(E)	*	See Fig. 2a (W), Fig. 3a (E)
WGAP.2, EGAP.2	GAP	Dominant @ 0.2°	7(W), 4(E)	*	See Fig. 2b (W), Fig. 3b (E)

* Each subcell represents a different land-cover type. Subcell fluxes were weighted according to each land-cover type's areal coverage within the 2.8° × 2.8° grid cell and then summed to obtain GCM grid cell fluxes.

to fully define the effects of land cover on surface fluxes, the stand-alone version used here describes the first-order direction and magnitude of effects and is efficient enough to permit a set of sensitivity experiments. A set of VBATS simulations (Table 1) was designed to address the last three questions (2, 3, 4) posed in section 1. We performed eight simulations for each of the GEAST and GWEST domains using the land-cover composition prescribed by the NC2, GAP, and EDC datasets at spatial resolutions of 2.8°, 0.4°, and 0.2° and the finest spatial resolution of each satellite-derived dataset (100 m and 1 km for GAP and EDC, respectively).

We examined the output from these simulations to quantify the effects of land cover on surface fluxes that are calculated for input to a GCM (net radiation, sensible and latent heat, and momentum). Runoff was also examined because of its importance in the water balance, as was ground heat flux because of its role in the surface energy balance.

2) ATMOSPHERIC FORCING FIELDS

In a stand-alone mode, VBATS requires downward shortwave and longwave radiation, specific humidity, air temperature, precipitation, surface pressure, and wind speed for each model time step. The Vegetation–Ecosystem Modeling and Analysis Project (VEMAP) database was used to provide a climatology of these variables for the two Wyoming GCM grid cells (Kittel et al. 1995). For our study, the VEMAP 0.5° × 0.5° daily climate data were extracted, averaged to 2.8° × 2.8° for each grid cell, and interpolated to hourly values as follows:

1) *Shortwave radiation.* The VEMAP fields of daily total incident solar radiation and mean daily irradiance were used to obtain hourly values of shortwave radiation. A sinusoidal variation of solar radiation was computed such that the area under its curve was equal to the daily total incident solar radiation.
2) *Air temperature.* The VEMAP fields of daily minimum temperature and daily maximum temperature were interpolated with a sine curve to create hourly values. The daily maximum temperature was assumed to occur at 1400 LT and the daily minimum temperature at one hour before sunrise.
3) *Surface pressure.* Surface pressure was not available in the VEMAP dataset. However, elevation was available at the VEMAP grid-cell resolution. This was used to compute an average elevation for both the GEAST and GWEST grid cells. Surface pressure was then computed using *U.S. Standard Atmosphere, 1976.* The pressure forcing was prescribed as a constant throughout the year.
4) *Specific humidity.* The VEMAP field of daily vapor pressure was used along with the surface pressure to compute a daily value of specific humidity. Specific humidity was prescribed as a constant for each day.
5) *Wind speed.* Wind speed was available from VEMAP as a monthly grid-averaged value at a 10-m height. The wind speed forcing was prescribed as a constant for each month.
6) *Precipitation.* The VEMAP field of daily precipitation was interpolated to obtain hourly precipitation. Daily precipitation was assumed to occur as a 12-h event during the cold season (October–March) and as a convective 2-h event in the warm season (April–September) (Seth et al. 1994). The sum of hourly precipitation was constrained to match the VEMAP daily values.
7) *Longwave radiation.* Longwave radiation was not available from the VEMAP dataset but was calculated based on atmospheric emissivity and the interpolated air temperature. Atmospheric emissivity was determined based on the VBATS formulation for cloudless skies (Brunt 1932) using the VEMAP daily vapor pressure. The effects of clouds on longwave radiation were included by assuming that clouds were present during precipitation events. Atmospheric emissivity was assigned a value of 0.95 during these times as per Seth et al. (1994).

The atmospheric forcing derived for each of the 2.8° × 2.8° grid cells was applied to each of the subcells identically.

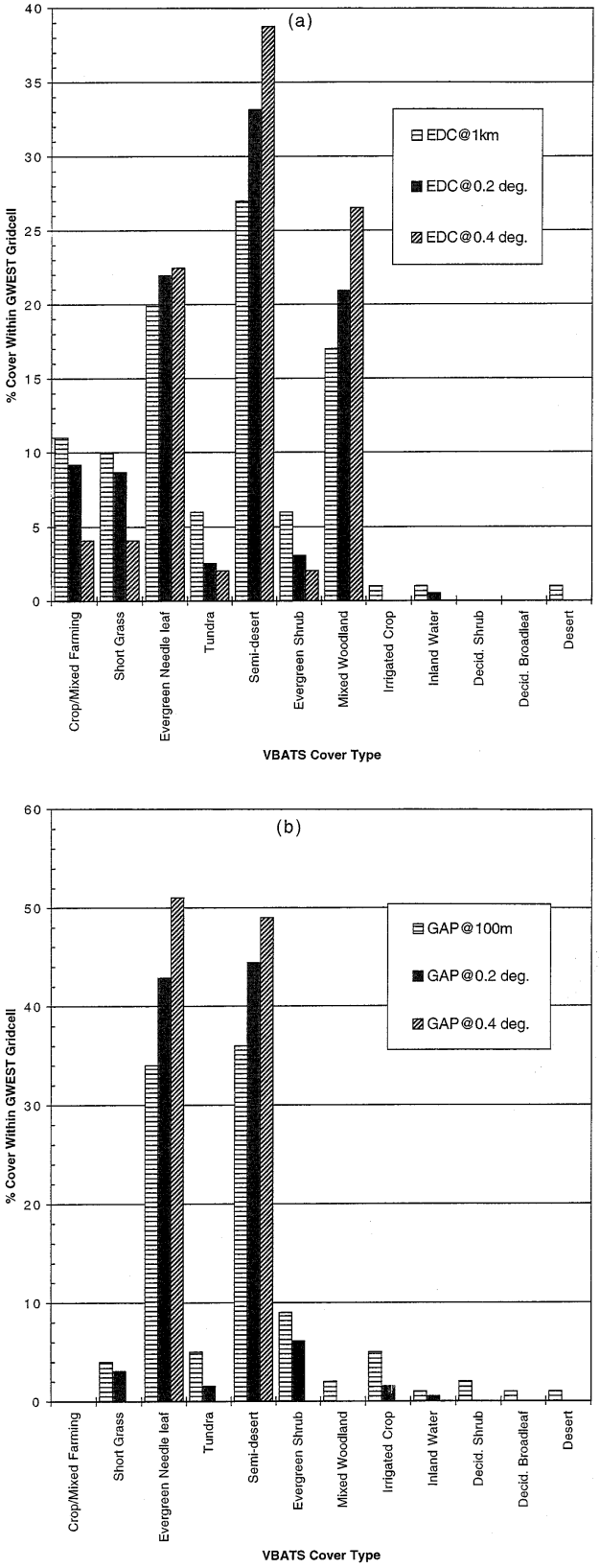

FIG. 2. VBATS land-cover types in the 2.8° × 2.8° western Wyoming GCM grid cell (GWEST) as prescribed by (a) the EDC dataset at resolutions of 1 km, 0.2°, and 0.4° and (b) the GAP dataset at resolutions of 100 m, 0.2°, and 0.4°. The NC2 dataset prescribes 100% evergreen needle leaf.

3) MODEL INITIALIZATION

Soil types are often associated with the type of overlying vegetation cover. While VBATS has the capability to also model heterogeneity in soil types simultaneously with land-cover heterogeneity (by specifying soil hydrologic and radiative properties according to texture and color types), we did not model this so that differences in surface fluxes could be attributed solely to differences in land cover. Soil texture and color were thus taken from the CCM2 prescribed fields for the GEAST and GWEST domains and identically assigned to all subcells. Inclusion of soil heterogeneity could alter the sensitivities described here.

Soil water in all subcells except inland water and irrigated crop (one or both of these types are present in most of the VBATS simulations listed in Table 1) was initialized at 50% of saturation. Inland water within VBATS is modeled as a saturated soil surface. Negative runoff is added to the subcell to replace water lost by evaporation and infiltration into deeper soil layers. Therefore, the soil water of inland water subcells was initialized at saturation. Irrigated crop is kept at field capacity via negative runoff, so soil water for irrigated crop subcells was initialized at field capacity. Soil temperatures were initialized at the mean air temperature for January, as were the foliage and canopy air temperatures. Snow cover and canopy water were initially set to zero.

Simulations were run for 20 years to allow the modeled soil water to equilibrate with the climatological forcings. No interannual variability was found during the last several years of each simulation so results were taken from the last year of each simulation.

3. Results

a. Comparison of the land-cover datasets

1) GWEST GRID CELL

The three datasets differ considerably in their depiction of the relatively diverse western grid cell. NC2 classifies the grid cell as the VBATS cover-type evergreen needle leaf. Although the full-resolution EDC and GAP datasets (EDC at 1 km and GAP at 100 m in Figs. 2a,b) have significant coverage of this type (20% and 34%, respectively), both are dominated instead by semidesert (27% and 36%). EDC contains a large (17%) mixed woodland component in addition to semidesert and evergreen needle leaf, while the GAP data is more evenly split between evergreen needle leaf and semidesert.

In general, as the EDC and GAP datasets are aggre-

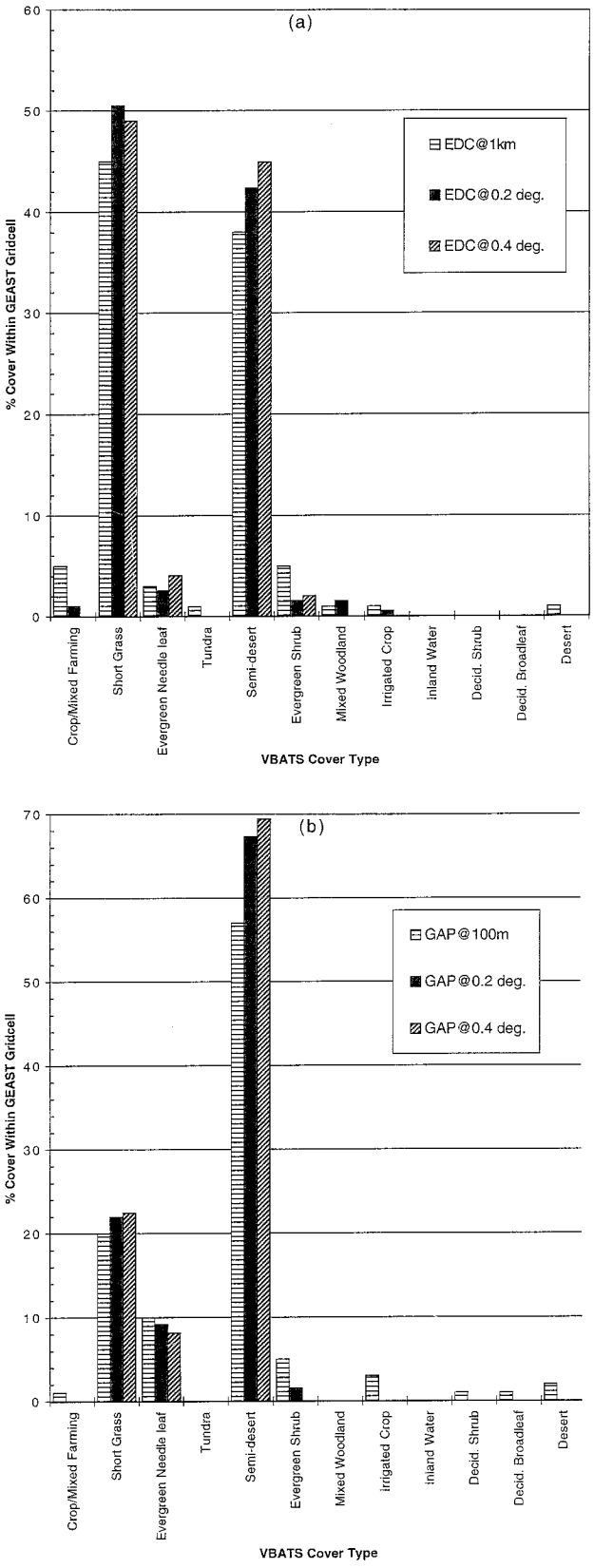

FIG. 3. VBATS land-cover types in the 2.8° × 2.8° eastern Wyoming GCM grid cell (GEAST) as prescribed by (a) the EDC dataset at resolutions of 1 km, 0.2°, and 0.4° and (b) the GAP dataset at resolutions of 100 m, 0.2°, and 0.4°. The NC2 dataset prescribes 100% short grass.

gated to coarser spatial resolutions (0.2° and 0.4°), the proportions of the two to three dominant cover types increase and the number of cover types within the grid cell decreases. The dominant cover type prescribed by the GAP dataset at 0.4° resolution changes from semidesert to evergreen needle leaf. The EDC dataset retains the largest number of VBATS land-cover types at coarser spatial resolutions. The EDC data at 0.4° resolution prescribes seven cover types, while the corresponding GAP data contains only two cover types. At a spatial resolution of 0.2°, the two datasets agree on the VBATS land-cover type for only 105 of 196 (54%) of the GWEST subcells. At 0.4° resolution, the agreement between the datasets increases to about 60% of the 49 subcells.

2) GEAST GRID CELL

All three land-cover datasets depict the GEAST grid cell as dominated by basin vegetation but differ in assignment of physiognomic dominance (Figs. 3a,b). The NC2 dataset prescribes short grass. The 1-km EDC data depict GEAST as a short-grass-dominated grid cell, although the data also contain a large (38%) semidesert component and some evergreen shrub and crop/mixed farming (5% each). In contrast, the 100-m GAP data are dominated by semidesert (58%), with a significant short-grass component (20%) and more evergreen needle leaf (10%) than EDC.

Resampling the GAP dataset to resolutions of 0.2° and 0.4° reduces the number of cover types and strengthens the dominance of semidesert within the grid cell. The number of VBATS cover types is reduced from nine in the full-resolution GAP dataset to three in the 0.4° data, and the proportion of semidesert increases to 70% of the grid cell. In the resampled EDC datasets, the codominance of semidesert and short grass also increases as resolution decreases. The number of cover types in the 0.2° and 0.4° EDC datasets is reduced to seven and four, respectively, from nine types at full (1 km) resolution. The agreement between datasets in the GEAST domain is similar to the results for GWEST. At a resolution of 0.2°, the GAP and EDC datasets correspond for 62% of the subcells. However, at 0.4° resolution, the agreement between datasets decreases to 59% of the subcells.

b. VBATS sensitivity to differences between NC2, EDC, and GAP dominant cover types

1) GWEST GRID CELL

Both the EDC and GAP datasets, when aggregated from their finest resolution to 2.8° × 2.8° using a dom-

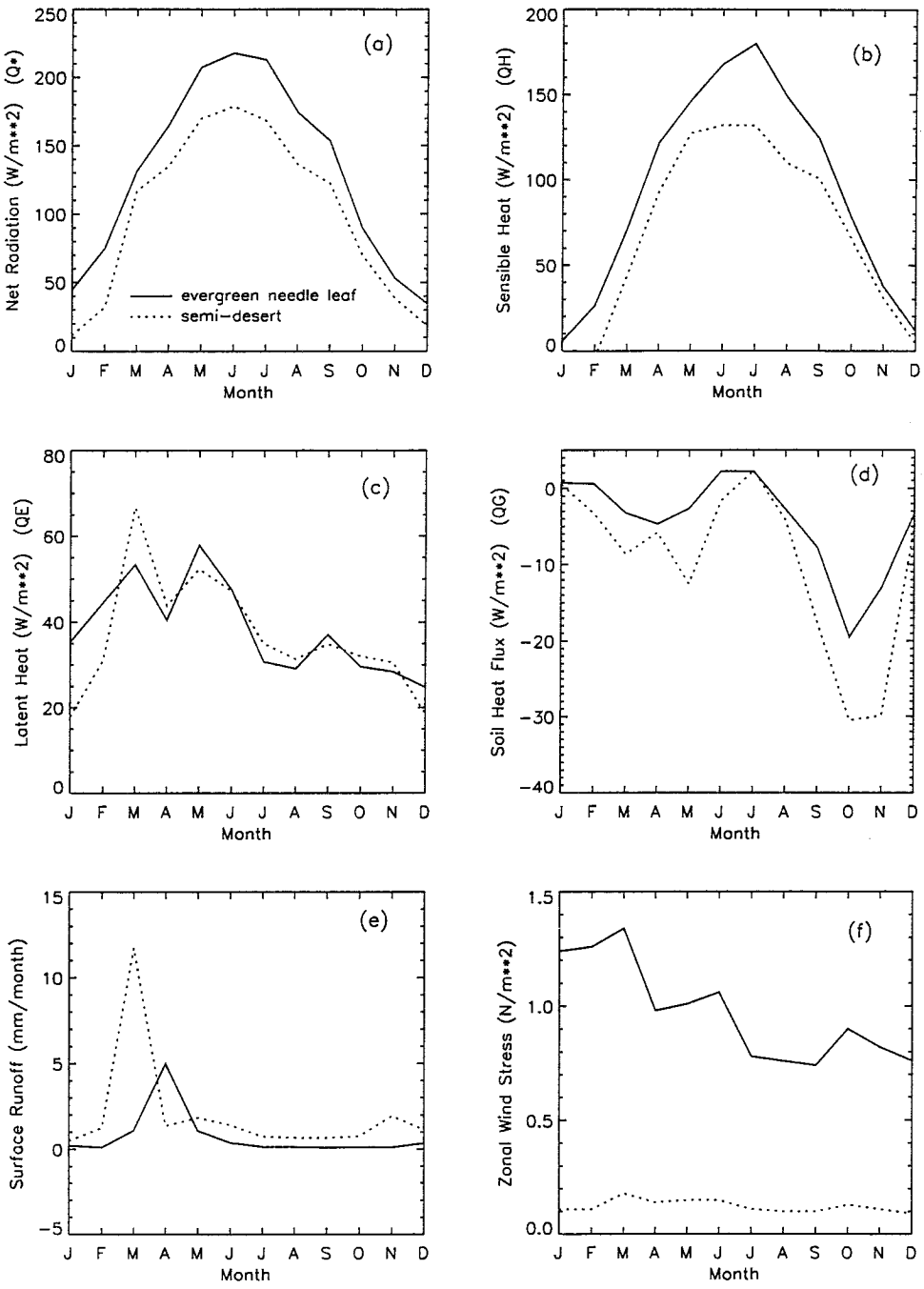

FIG. 4. Results from GWEST VBATS simulations at 2.8° spatial resolution: WEN (100% evergreen needle leaf) and WSD (100% semidesert). Monthly averages of (a) net radiation, (b) sensible heat, (c) latent heat, (d) soil heat flux, (e) total runoff, and (f) zonal wind stress. Fluxes are positive away from the surface.

inant-cover-type rule, prescribed semidesert in the GWEST domain while the NC2 dataset prescribed evergreen needle leaf. To quantify the effects of this difference in terms of VBATS simulated surface fluxes, we compared output from the WEN (100% evergreen needle leaf) and WSD (100% semidesert) simulations (Table 1).

The semidesert average monthly net radiation Q^* was consistently lower than the evergreen needle leaf Q^*, up to a maximum difference of 45 W m^{-2} in July (about 23% lower for the annual average) (Fig. 4a, Table 2). Semidesert soil surface and leaf temperatures were higher than corresponding evergreen needle leaf temperatures (~3°–5°C), particularly in the summer months,

TABLE 2. Annual averages for GWEST and GEAST simulations at 2.8° spatial resolution. Fluxes (QH, QE, QG) are positive away from the surface. Land-cover types shown below represent 100% of the grid cell. Values on GWEST second rows are percent differences from WEN simulation, while those on GEAST second rows are differences from ESG simulation. See Table 1 for a description of each simulation.

	WEN (Evergreen needle leaf)	WSD (semi-desert)	ESG (Short grass)	ESD (Semi-desert)
Net radiation (Q^*)	129.9	99.9	100.3	94.4
(W m^{-2})	—	−23.1%	—	−5.9%
Sensible heat (QH)	93.2	68.7	72.9	71.2
(W m^{-2})	—	−26.3%	—	−2.3%
Latent heat (QE)	38.2	36.8	30.3	29.4
(W m^{-2})	—	−3.7%	—	−3.0%
Soil heat flux (QG)	−4.3	−9.7	−3.7	−9.6
(W m^{-2})	—	+125.6%	—	+159.5%
Total runoff	0.73	2.00	0.29	0.79
(mm month^{-1})	—	+174.0%	—	+172.4%
Zonal wind stress	0.97	0.12	0.14	0.13
(N m^{-2})	—	−87.6%	—	−7.1%

which resulted in a slight increase in the upward longwave radiation (not shown). This accounted for a decrease in Q^* in these months. A more significant effect on Q^* throughout the year was the decrease in semidesert Q^* resulting from the higher prescribed albedo of the semidesert cover type (0.25 versus 0.14 for evergreen needle leaf).

On an annual basis, the lower semidesert Q^* was partitioned into a lower sensible heat flux (QH), slightly lower latent heat flux (QE), and a doubling of ground heat flux (QG) (Table 2). Within VBATS, the important differences between the semidesert and evergreen needle leaf parameterizations, besides albedo, are a high fractional vegetation cover for evergreen needle leaf (0.7–0.8) compared to semidesert (0.0–0.1), a smaller prescribed seasonality in LAI for evergreen needle leaf, and a larger roughness length for evergreen needle leaf (1.0 m) compared to semidesert (0.1 m). Due to the relatively dry climate forcings (average monthly precipitation was less than 30 mm), the significance of the interaction of moisture with vegetation (interception, transpiration) was greatly reduced. Hence, because of the lack of available moisture, predicted QE differed by only a small amount annually (1.4 W m^{-2}) despite the large difference in vegetation cover. The annual difference between semidesert and evergreen needle leaf Q^* was therefore primarily accounted for by QH.

The characteristics of the evergreen needle leaf QE were peaks in March and May, a trough in April, and a generally flat profile in July–November (Fig. 4c). Generally, this profile followed that of the GWEST precipitation seasonality (not shown), with the exception being the peak in March, which was driven by substantial snow melt and subsequent ground evaporation. The predicted snow pack decreased from 43 mm of water in February to 18 mm in March (not shown).

Semidesert QE was most different from that of evergreen needle leaf QE in January–March, with the differences in other months being less than 6 W m^{-2} (Fig. 4c). The differences in January–March can be seen most clearly by dividing the modeled evapotranspiration into components of transpiration, intercepted leaf evaporation, and ground evaporation (Fig. 5). In January and February when there was no transpiration for either land-cover type, ground evaporation was similar and snowmelt was minimal, the semidesert evapotranspiration was less than that for evergreen needle leaf primarily because of the near-zero intercepted leaf evaporation (Fig. 5d). In March, transpiration was still not important in the water balance, but the semidesert ground evaporation became much larger than the evergreen needle leaf ground evaporation and more than offset the decreased intercepted leaf evaporation. For other months (April–December), the smaller semidesert transpiration and intercepted leaf evaporation was balanced for the most part by the increase in ground evaporation. As a result, under these climatic forcings, the semidesert QE was quite similar to the evergreen needle leaf QE during the months of April–December.

The magnitude of the evergreen needle leaf QG was less than 5 W m^{-2} for all months except September to November when there was increased heat flux from the deeper layers of the soil to the surface as the surface soil cooled (Fig. 4d). The semidesert QG was a more significant component of the energy balance than the evergreen needle leaf QG because of the lower fraction of vegetation cover in semidesert.

Runoff amounts for evergreen needle leaf were near zero for all months except March–May (Fig. 4e). The peak in April occurred when the surface soil water was at a maximum for the year due to snowmelt and subsequent infiltration. The peak runoff for semidesert came one month earlier and was larger than the evergreen needle leaf runoff peak. The relative lack of vegetation in the semidesert cover type allowed more precipitation to reach the ground and increased the surface soil water more quickly than in the evergreen needle leaf simulation. Surface soil water for semidesert peaked one month earlier (not shown). Consequently, snowmelt and further precipitation combined to create an earlier runoff peak.

Since the wind forcings were identical in both simulations, the average zonal wind stress for a given month was primarily affected by differences in surface roughness. The effective surface roughness of the semidesert cover type is essentially that of bare soil and is much smoother than that of evergreen needle leaf. Consequently, zonal wind stress was significantly lower in the semidesert simulation (Fig. 4f).

2) GEAST GRID CELL

In the GEAST domain, at 2.8° resolution, the NC2 and EDC datasets prescribe short grass while the GAP

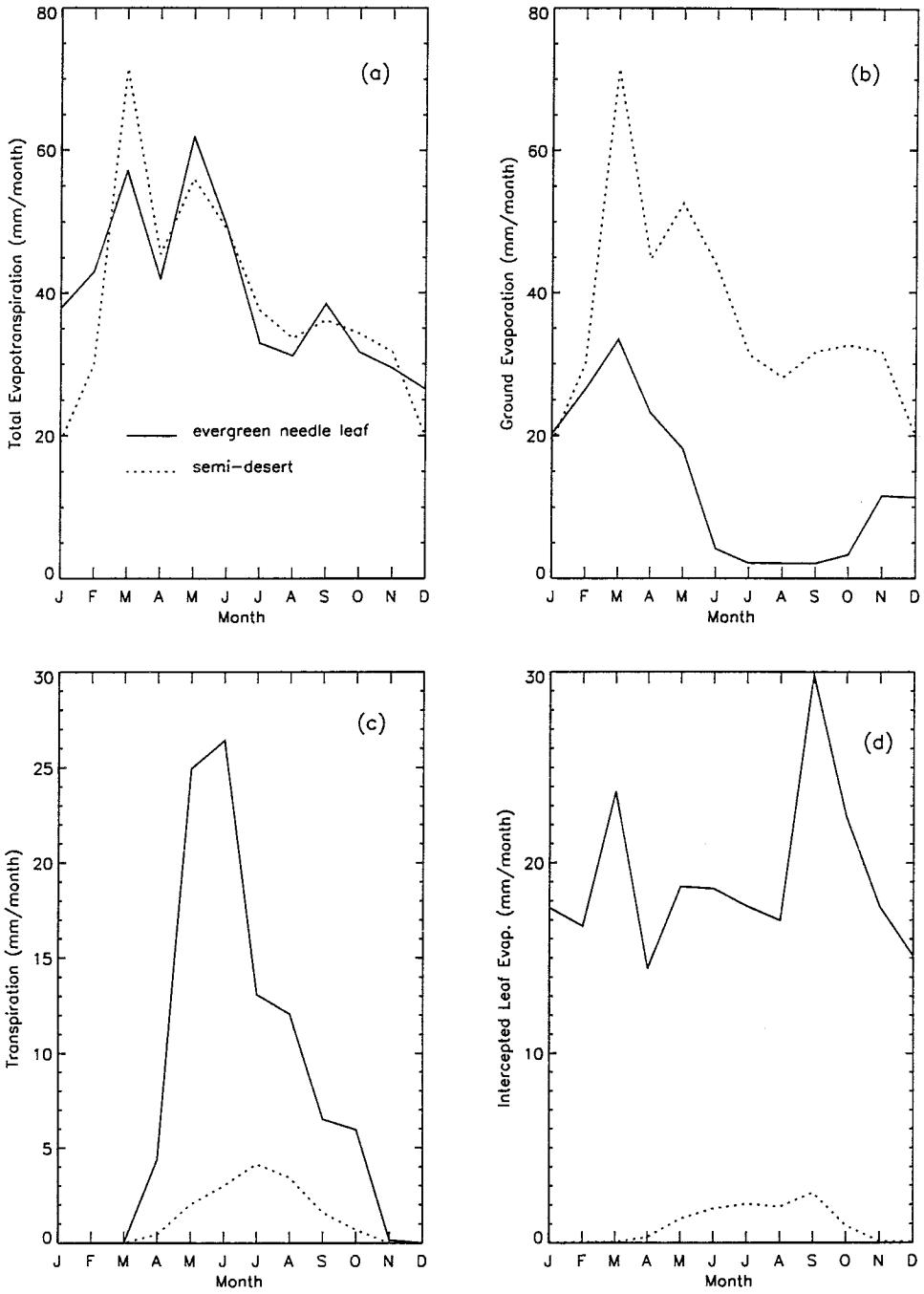

FIG. 5. Results from GWEST VBATS simulations at 2.8° spatial resolution: WEN (100% evergreen needle leaf) and WSD (100% semidesert). Monthly averages of (a) total evapotranspiration, (b) ground evaporation, (c) transpiration, and (d) intercepted leaf evaporation.

dataset prescribes semidesert as the dominant cover type. Therefore, we compared output from the ESG (100% short grass) and ESD (100% semidesert) simulations (Table 1).

Semidesert Q^* was lower than short grass Q^* by no greater than 10 W m^{-2} in any month (Fig. 6a) and by less than 6% for the annual average (Table 2), indicating that these two cover types influence net radiation similarly for these climatic forcings. The smaller Q^* of semidesert resulted in a smaller QH than short grass in most months (Fig. 6b), while monthly QE was mostly unchanged ($<$3 W m^{-2}), except in July ($\sim$8 W m^{-2}) (Fig. 6c). The 8 W m^{-2} decrease in semidesert Q^* appears to be due to the difference between the simulated

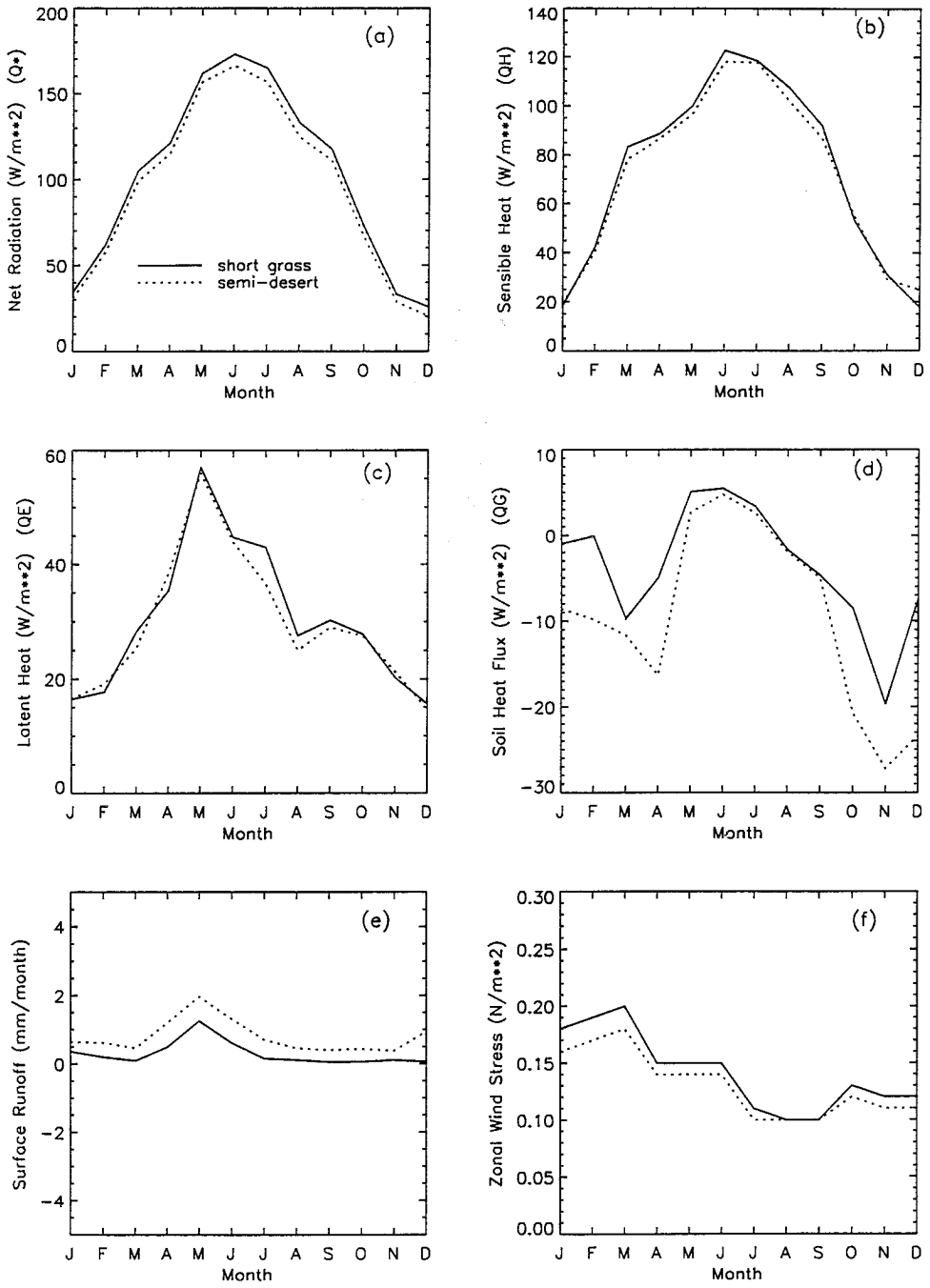

FIG. 6. Results from GEAST VBATS simulations at 2.8° spatial resolution: ESG (100% short grass) and ESD (100% semidesert). Monthly averages of (a) net radiation, (b) sensible heat, (c) latent heat, (d) soil heat flux, (e) total runoff, and (f) zonal wind stress. Fluxes are positive away from the surface.

transpiration for this month. The maximum difference in transpiration between these two simulations occurred in July, the month of peak transpiration for both cover types.

The VBATS parameterizations of short grass and semidesert are quite similar in most respects. Of the 14 biophysical parameters that represent each cover type, only two (maximum fractional vegetation cover and maximum LAI) are notably different between cover types. Semidesert is parameterized by a small maximum fractional vegetation cover (0.1 versus 0.8 for short grass) and high maximum LAI (6 versus 2 for short grass). The results indicate that for these atmospheric forcings, the combination of high LAI and low

fractional vegetation cover produces nearly the same surface fluxes as low LAI and high fractional vegetation cover.

The larger proportion of bare soil in the semidesert cover type resulted in a larger QG contribution during the cold season, although it was still a small proportion of the total energy budget (Fig. 6d). Runoff for the semidesert simulation was slightly increased over that of the short grass simulation because of the difference in fractional vegetation cover (Fig. 6e). Zonal wind stress was virtually identical (<0.02 N m^{-2} difference) for the two simulations (Fig. 6f).

c. *VBATS sensitivity to differences between full resolution EDC and GAP datasets*

1) GWEST GRID CELL

Despite the substantial differences in land cover prescribed by the full-resolution EDC (WEDC.FR) and GAP (WGAP.FR) datasets (compare Fig. 2a with Fig. 2b), the simulated monthly fluxes were similar except in the summer months (Fig. 7). Annually, the WGAP.FR simulations of Q^*, QH, and QG differed from the corresponding WEDC.FR quantities by 0.6, 1.6, and 0.3 W m^{-2}, respectively (Fig. 8). The annual difference in QE was about 2.5 W m^{-2}, but the monthly differences in QE were up to 8 W m^{-2} in the summer months.

An analysis of the subcell fluxes revealed that the difference in QE between the two datasets was primarily related to the relative proportions of the wet cover types (inland water and irrigated crop) prescribed by each of the satellite-derived datasets (Fig. 2a and Fig. 2b). The GAP and EDC datasets classify 6% and 2% of the grid cell, with soil water maintained either at saturation or at field capacity, respectively. In the dry climatic conditions considered here, even small proportions of these wet cover types substantially increased the availability of moisture in the grid cell. Consequently, the larger proportions of wet cover types in the GAP dataset relative to the EDC dataset caused a higher QE in months when energy was present to evaporate the increased available moisture. The aggregated contribution of the other cover types to the grid-cell QE was effectively the same for both datasets.

Monthly runoff amounts were also noticeably different between the two simulations due to the proportions of these two wet cover types, particularly during the summer months (Fig. 7e). Both wet cover types require water (supplied by negative runoff in VBATS) to make up for losses from evaporation and soil infiltration. Due to the small runoff amounts from the other subcells, the overall grid cell runoff was dominated by negative runoff from subcells containing these two cover types.

The land-cover differences between the two datasets did not significantly affect the monthly zonal wind stress (Fig. 7f). The annual difference was about 0.03 N m^{-2} (Fig. 8).

2) GEAST GRID CELL

In the GEAST domain, VBATS was even less sensitive to the differences in satellite-derived land cover than in the GWEST domain. The annual averages of Q^*, QH, QE, and QG differed by at most 1.5 W m^{-2} (Fig. 9). Monthly differences of these quantities were consistently small (not shown). This is primarily because the grid cell is dominated by two cover types (short grass and semidesert) that influence surface fluxes similarly in these simulations (see section 3b) and because the wet cover types only occupy 3% and 1% of the GAP and EDC grid-cell land cover, respectively (about one-half that of GWEST wet land cover). Runoff again differed between the two datasets because of the inland water and irrigated crop cover types, although not quite as much as in the GWEST domain (Fig. 9). Annual zonal wind stress values differed by 0.06 N m^{-2} (Fig. 9).

d. *VBATS sensitivity to coarser prescriptions of land cover*

Reductions in dataset spatial resolution decreased the number of cover types in each grid cell, with different results depending on the dataset. Here we compare the output from the full-resolution simulations to simulations that use reduced resolution versions of the datasets.

1) GWEST GRID CELL

Average annual Q^* was slightly higher for both the GAP and EDC datasets at coarse spatial resolution than at finer spatial resolution (Fig. 8). The QH increased and QE decreased as the number of cover types were reduced with aggregation. The changes in QH and QE were largest in the months of April through October (not shown). Part of the reduction in QE and, therefore, some of the increase in QH during these months can be attributed to the reduction or elimination of the irrigated crop and inland water cover types in the coarser-resolution datasets. The reduction in QE was largest for the GAP dataset, which at full resolution had the largest wet cover type component (6%). In the winter months, snow and cold temperatures combined to reduce the effects of the wet cover types and of differences in vegetated land cover on QE at the various spatial resolutions. During these months, transpiration was zero and evaporation from both soil and water surfaces was suppressed by the snow cover and by the low amount of energy available at the surface.

Runoff was substantially affected by the wet cover types with the greatest increase in grid-cell runoff occurring in the GAP datasets as the wet cover types were reduced or eliminated (Fig. 8). Annually averaged zonal

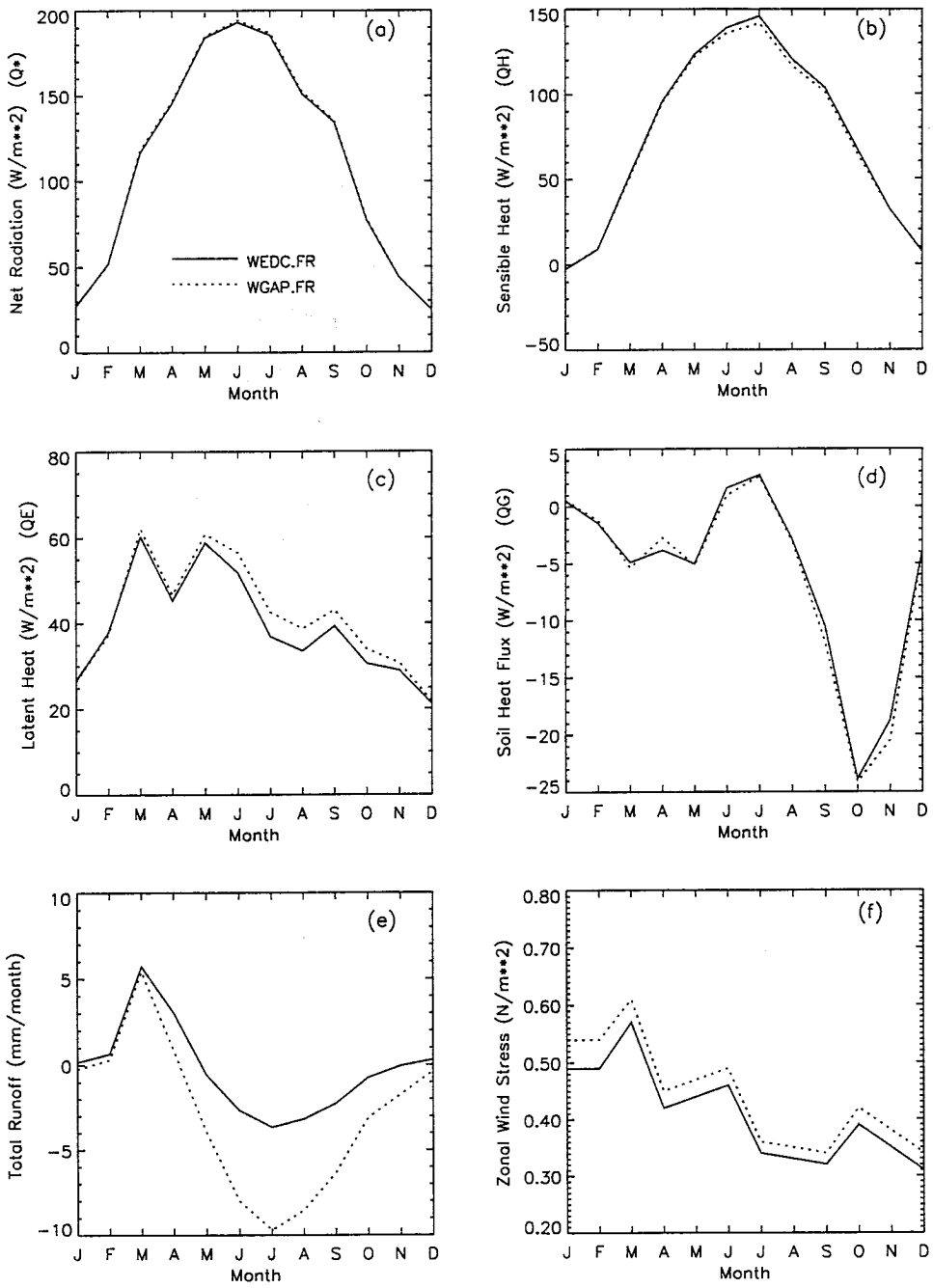

FIG. 7. Results from GWEST VBATS simulations using the full-resolution EDC (WEDC.FR) and GAP (WGAP.FR) land-cover datasets. Monthly averages of (a) net radiation, (b) sensible heat, (c) latent heat, (d) soil heat flux, (e) total runoff, and (f) zonal wind stress. Fluxes are positive away from the surface.

wind stresses differed by 0.07 and 0.12 N m^{-2} between the EDC and GAP full and 0.4° resolution datasets, respectively (Fig. 8).

2) GEAST GRID CELL

The relative homogeneity of the land cover and the smaller proportion of wet cover types in the GEAST domain resulted in less significant flux differences as the spatial resolutions of the EDC and GAP datasets were reduced. Annual Q^*, QH, QE, and QG fluxes differed by at most 1.1 W m^{-2} between the EDC full-resolution simulation (EEDC.FR) and the coarsest resolution EDC dataset (EEDC.4) (Fig. 9). For the GAP datasets, the magnitude of the differences in Q^*, QH, and QG were similar to those for the EDC data. Dif-

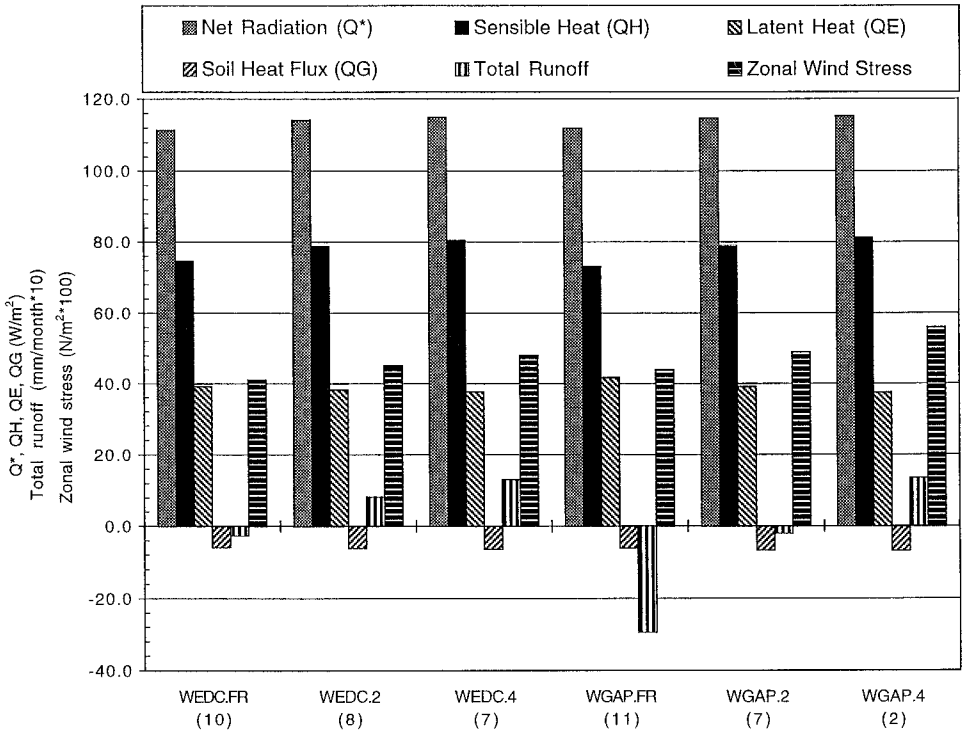

FIG. 8. Annual averages for GWEST simulations at dataset spatial resolutions of 100 m (WGAP.FR), 1 km (WEDC.FR), 0.2° (WEDC.2, WGAP.2), and 0.4° (WEDC.4, WGAP.4). Fluxes are positive away from the surface. Runoff values are multiplied by 10.0. Wind stress values are multiplied by 100.0. Numbers in parentheses on *x*-axis labels are the number of cover types prescribed by each dataset. See Table 1 for a description of each simulation.

ferences in QE were larger due to the elimination of wet cover types in the coarser-resolution GAP datasets.

The runoff differences were smaller than in GWEST but were still substantial, particularly for the GAP datasets, again due to the irrigated crop and inland water cover types (Fig. 9). Zonal wind stress differences were negligible between the EDC datasets and small (<0.03 N m^{-2}) for the GAP datasets (Fig. 9).

4. Discussion

The nature of GWEST land cover prescribed by the satellite datasets at full resolution illustrates a disadvantage of aggregating by dominant cover type. The dominance of the semidesert cover type in GWEST as prescribed by the EDC and GAP datasets is weak. Evergreen needle leaf and mixed woodland also occupy substantial proportions of the grid cell (20% and 17%, respectively, for the EDC dataset, and 34% and 2% for the GAP dataset) and are very similar with respect to most VBATS biophysical parameters. Taken together, these two cover types as prescribed by the GAP dataset roughly equal the proportion of semidesert within the grid cell. For the EDC dataset, the sum of these two cover types dominates over semidesert. Consequently, an alternate choice for the GCM grid cell could be evergreen needle leaf, as in the NC2 prescription. This choice between two dominant cover types is important here because of the distinctly different effects of the semidesert and evergreen needle leaf cover types on surface fluxes (see Fig. 4). It is clear that the biophysical parameters associated with land-cover types must be considered when producing GCM-scale land-cover maps from satellite data. Recently, a new classification scheme has been proposed that characterizes land cover according to primary characteristics of vegetation structure in contrast to a traditional taxonomic or floristic approach (Running et al. 1995). Further, DeFries et al. (1995) propose replacing discrete vegetation classes with a set of continuous land surface characteristics. This latter approach would eliminate the need for assigning a single or even multiple land-cover types to a grid cell but would require new model parameterizations based on these continuous characteristics.

The sensitivity of these VBATS simulations to small proportions of wet cover types (e.g., inland water and irrigated crop) emphasizes that the consequences of ignoring the potential contribution of certain cover types to the relative distribution of surface fluxes can often be disproportionate with respect to their areal coverage within the grid cell. Land surface parameterizations have advanced to the point where GCM grid-cell land cover can now be modeled using more than one land-

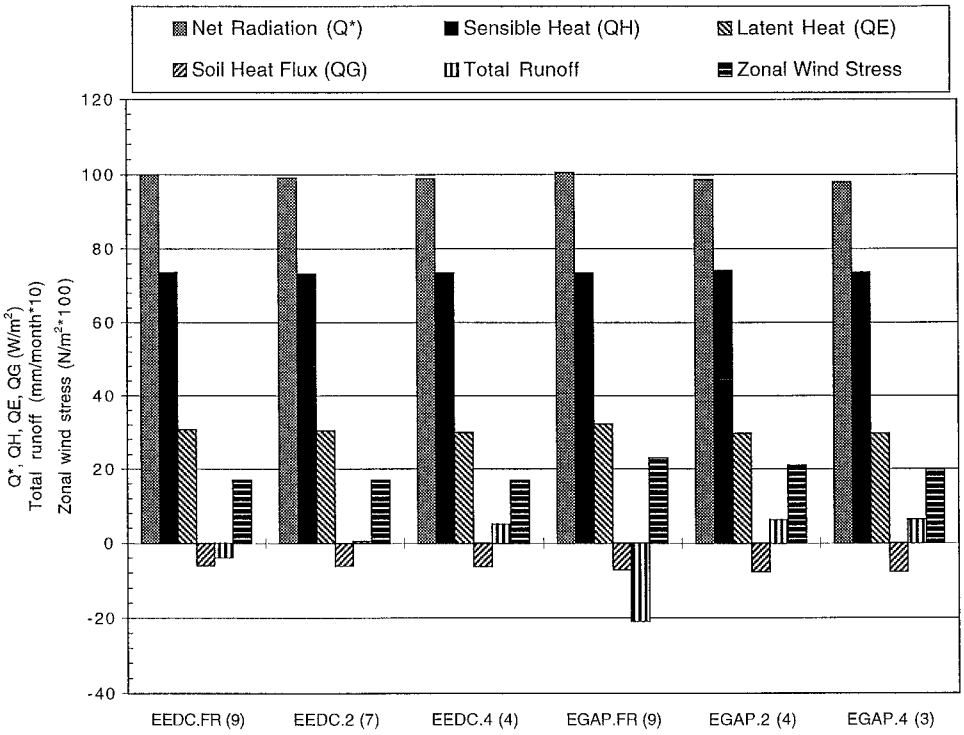

FIG. 9. Annual averages for GEAST simulations at dataset spatial resolutions of 100 m (EGAP.FR), 1 km (EEDC.FR), 0.2° (EEDC.2, EGAP.2), and 0.4° (EEDC.4, EGAP.4). Fluxes are positive away from the surface. Runoff values are multiplied by 10.0. Wind stress values are multiplied by 100.0. Numbers in parentheses on *x*-axis labels are the number of cover types prescribed by each dataset. See Table 1 for a description of each simulation.

cover type [e.g., the Land Surface Model (LSM); Bonan 1996]. The choice of how many and which cover types to use should be evaluated with respect to the land-cover composition within the grid cell and each cover type's response to the range of atmospheric forcing it might experience.

It is necessary to address the question of whether the differences in surface fluxes reported here that result from different representations of land cover would have any effects on climate. First, we briefly consider the potential impact of differences between current and satellite-derived land cover on climate simulations that use the traditional approach to modeling land cover, namely the assignment of a single dominant land-cover type to a GCM grid cell. The choice of a dominant land-cover type can have significant effects on the net radiation at the land surface and the subsequent partitioning into sensible and latent heat fluxes (e.g., the choice between evergreen needle leaf and semidesert in the GWEST grid cell) (Table 2). GCM studies of the effects of deforestation have shown that the simulated regional climate is modified significantly by the conversion of tropical forest to secondary vegetation (as summarized by Henderson-Sellers et al. 1993). For example, Dickinson and Kennedy (1992) simulated large decreases in regional precipitation resulting from initial changes (before atmospheric and surface feedbacks) of 34 W m^{-2} in surface radiative forcing due to differences in land-cover albedo and roughness. Hence, it is not unrealistic to expect that the choice of the dominant cover type in the GWEST grid cell could have some effect on the simulated regional climate.

Second, we consider the effects of differences in land cover if land-cover heterogeneity is modeled to some limited extent. It is possible that the choices among the land-cover prescriptions represented by the various spatial versions of the satellite-derived datasets may not matter a great deal when used in climate simulations under the assumptions made in the modeling approach used here (Fig. 8 and Fig. 9). Maximum differences in annual net radiation and sensible and latent heat fluxes are on the order of a few watts per square meter. However, in GWEST, the values of surface fluxes obtained using these heterogeneous land-cover representations (Fig. 8) differ substantially from the homogeneous representation (Table 2). For example, the simulated annual average of net surface radiative forcing using the WEDC.FR dataset is 111 W m^{-2}, while use of the NC2 dominant cover type results in a value of 130 W m^{-2}. Again, based on the magnitude of this difference, it would be reasonable to expect that the simulated regional climate could be affected. Further support for this is offered in a recent regional modeling study of the effects of potential versus current vegetation distri-

butions on United States regional climates (Copeland et al. 1996). By comparing regional climate model simulations using potential and satellite-derived vegetation distributions, they suggested that current land use has resulted in warmer and wetter summertime surface conditions in certain United States regional areas. For example, the conversion of land cover from short-grass prairie to crop/mixed farming in the central plains resulted in a 5% decrease in simulated precipitation in this region.

It is important to note two important limitations of this type of modeling with respect to predicting the behavior of land surface parameterizations within GCMs. First, the effects of atmospheric feedback are ignored in these simulations. These effects can be positive or negative, though coupled experiments generally produce lower sensitivities than uncoupled ones (Henderson-Sellers 1993).

Second, the relevance of the model sensitivities described here to the potential behavior of LSPs within GCMs is restricted to applications that do not consider the influences of subgrid atmospheric forcing. In our simulations, we have applied the same mean grid climate forcing to all subcells. The application of a more realistic distribution of atmospheric forcings to the subcells would alter the sensitivities described here. In particular, although the average yearly Wyoming precipitation derived from VEMAP data compares favorably with the 30-yr climatology for the state described by Martner (1986), the significant spatial variability in precipitation is not represented here. VBATS's sensitivity to differences in satellite-derived land cover could be significantly affected by considering this spatial variability in precipitation. By applying the average precipitation forcing to all subcells, those with the most vegetation (e.g., evergreen needle leaf) tend to receive a smaller amount of precipitation than might normally be expected, while semidesert subcells could receive more precipitation than normal. This could minimize differences in controls on surface fluxes by these two land-cover types. Several investigators are exploring the sensitivity of land surface parameterizations to subgrid climate forcing with both stand-alone and coupled simulations (e.g., Entekhabi and Eagleson 1989; Pitman 1991; Pitman et al. 1993; Seth et al. 1994).

5. Conclusions

Comparison of two satellite-derived land-cover datasets with a standard map–atlas-based dataset commonly used in GCMs revealed substantial differences in the areal proportions of land-cover types within two $2.8° \times 2.8°$ Wyoming GCM grid cells. Aggregation of the satellite-derived land-cover data to the GCM grid cell resolution resulted in a different designation of land cover for both grid cells than is used in the standard map–atlas product. In the western grid cell, this resulted in substantial differences in the magnitudes of surface fluxes simulated by a land surface parameterization scheme. In the eastern grid cell, the resulting differences in surface fluxes were smaller because of the similar biophysical parameterization of the two dominant cover types prescribed by the datasets. These results support the assertion that accurate satellite-derived land-cover datasets are needed to improve prescriptions of land cover within current GCMs (Townshend et al. 1991).

Our results also support other studies suggesting that land-cover heterogeneity needs to be considered when modeling the effects of the land surface on climate (Avissar and Pielke 1989; Bonan et al. 1993; Henderson-Sellers and Pitman 1992). For these Wyoming GCM grid cells, land-cover heterogeneity effects on average annual sensible and latent heat fluxes may be reasonably modeled (less than 10% difference from fluxes calculated by the model using the land-cover data at its finest spatial resolution) by accounting for the presence of a relatively small number of cover types (under the assumption that subgrid scale fluxes can be combined linearly). Recently developed land surface parameterizations have the capability to account for this extent of within-cell land-cover heterogeneity (e.g., Bonan 1996).

The simulations performed here also suggest that for arid regions, the partitioning of net radiation into sensible and latent heat fluxes is influenced by relatively small proportions of ''wet'' cover types (e.g., inland water and irrigated crop) within the grid cell. Therefore, some consideration should be given to including wet cover types when modeling the grid-cell land cover in arid regions.

In general, these results suggest that the value of high-resolution land-cover datasets depends on the presence of certain critical land-cover types and on the biophysical differences among other types. Land-cover classification schemes for climate modeling should ideally be flexible in terms of spatial resolution and information content to take account of model sensitivities to different surface conditions. The simplest way of achieving this flexibility would be to maintain as fine a spatial resolution and as detailed a classification scheme as possible in the archived land surface products. This would of course increase data processing and storage requirements.

Acknowledgments. The authors would like to acknowledge the financial support of NASA's Earth Observing System (EOS) program as part of one of its InterDisciplinary Science (IDS) teams (Principal Investigator R. Dickinson). K. W. Oleson was supported in part by a grant from the National Science Foundation (NSF) (No. BIR-9413218). The authors express their appreciation to N. Rosenbloom and T. Kittel for providing information pertaining to the VEMAP dataset. The reviewers are thanked for insightful comments that helped clarify this manuscript. We also thank Anji Seth for commenting on an earlier draft of this manuscript.

REFERENCES

Avissar, R., 1992: Conceptual aspects of a statistical–dynamical approach to represent landscape subgrid-scale heterogeneities in atmospheric models. *J. Geophys. Res.,* **97,** 2729–2742.

——, and R. A. Pielke, 1989: A parameterization of heterogeneous land surfaces for atmospheric numerical models and its impact on regional meteorology. *Mon. Wea. Rev.,* **117,** 2113–2136.

Blackstone, D. L., Jr., 1988: Traveler's guide to the geology of Wyoming. Geological Survey of Wyoming Bulletin 67, 130 pp. [Available from Geological Survey of Wyoming, University of Wyoming, Laramie, WY 82701.]

Bonan, G. B., 1996: A land surface model (LSM version 1.0) for ecological, hydrological, and atmospheric studies: Technical description and user's guide. NCAR Tech. Note NCAR/TN-417+STR, 150 pp. [Available from NCAR Education and Outreach Program, P.O. Box 3000, Boulder, CO, 80307.]

——, D. Pollard, and S. L. Thompson, 1993: Influence of subgrid-scale heterogeneity in leaf area index, stomatal resistance, and soil moisture on grid-scale land–atmosphere interactions. *J. Climate,* **6,** 1882–1897.

Brown, J. F., T. R. Loveland, J. W. Merchant, B. L. Reed, and D. O. Ohlen, 1993: Using multisource data in global landcover characterization: Concepts, requirements, and methods. *Photogramm. Eng. Remote Sens.,* **59,** 977–987.

Brunt, D., 1932: Notes on radiation in the atmosphere. *Quart. J. Roy. Meteor. Soc.,* **58,** 389–420.

Coleman, T. L., L. Gudapati, and J. Derrington, 1990: Monitoring forest plantations using landsat thematic mapper data. *Remote Sens. Environ.,* **33,** 211–221.

Collins, D. C., and R. Avissar, 1994: An evaluation with the Fourier amplitude sensitivity test (FAST) of which land-surface parameters are of greatest importance in atmospheric modeling. *J. Climate,* **7,** 681–703.

Copeland, J. H., R. A. Pielke, and T. G. F. Kittel, 1996: Potential climatic impacts of vegetation change: A regional modeling study. *J. Geophys. Res.,* **101,** 7409–7418.

Davis, F. W., D. M. Stoms, J. E. Estes, J. Scepan, and J. M. Scott, 1990: An information systems approach to the preservation of biological diversity. *Int. J. Geogr. Info. Syst.,* **4,** 55–78.

DeFries, R. S., and J. R. G. Townshend, 1994: NDVI-derived land cover classifications at a global scale. *Int. J. Remote Sens.,* **15,** 3567–3586.

——, and Coauthors, 1995: Mapping the land surface for global atmosphere–biosphere models: Toward continuous distributions of vegetation's functional properties. *J. Geophys. Res.,* **100,** 20 867–20 882.

Dickinson, R. E., 1988: The force-restore model for surface temperature and its generalizations. *J. Climate,* **1,** 1086–1097.

——, and P. J. Kennedy, 1992: Impacts on regional climate of Amazon deforestation. *Geophys. Res. Lett.,* **19,** 1947–1950.

——, A. Henderson-Sellers, and P. J. Kennedy, 1993: Biosphere–Atmosphere Transfer Scheme (BATS) Version 1e as coupled to the NCAR Community Climate Model. NCAR Tech. Note NCAR/TN-387+STR, 72 pp. [Available from NCAR Education and Outreach Program, P.O. Box 3000, Boulder, CO, 80307.]

Driese, K. L., W. A. Reiners, E. H. Merrill, and K. Gerow, 1996: A digital land cover map of Wyoming: A tool for vegetation analysis. *J. Veg. Sci.,* in press.

Entekhabi, D., and P. Eagleson, 1989: Land surface hydrology parameterization for the atmospheric general circulation models including subgrid-scale spatial variability. *J. Climate,* **2,** 816–831.

Goward, S. N., C. J. Tucker, and D. G. Dye, 1985: North American vegetation patterns observed with the NOAA-7 Advanced Very High Resolution Radiometer. *Vegetatio,* **64,** 3–14.

Hall, F. G., J. R. Townshend, and E. T. Engman, 1995: Status of remote sensing algorithms for estimation of land surface state parameters. *Remote Sens. Environ.,* **51,** 138–156.

Henderson-Sellers, A., 1993: A factorial assessment of the sensitivity of the BATS land-surface parameterization scheme. *J. Climate,* **6,** 227–247.

——, and A. J. Pitman, 1992: Land-surface schemes for future climate models: Specification, aggregation, and heterogeneity. *J. Geophys. Res.,* **97,** 2687–2696.

——, R. E. Dickinson, T. B. Durbidge, P. J. Kennedy, K. McGuffie, and A. J. Pitman, 1993: Tropical deforestation: Modeling local to regional scale climate change. *J. Geophys. Res.,* **98,** 7289–7315.

Hopkins, P. F., A. L. Maclean, and T. Liliesand, 1988: Assessment of thematic mapper imagery for forest applications under lake states conditions. *Photogramm. Eng. Remote Sens.,* **54,** 61–68.

Kittel, T. G. F., N. A. Rosenbloom, T. H. Painter, D. S. Schimel, and VEMAP Modeling Participants, 1995: The VEMAP integrated database for modeling United States ecosystem/vegetation sensitivity to climate change. *J. Biogeography,* **22,** 857–862.

Knight, D. H., 1994: *Mountains and Plains: The Ecology of Wyoming Landscapes.* Yale University Press, 338 pp.

Koster, R. D., and M. J. Suarez, 1992: Modeling the land surface boundary in climate models as a composite of independent vegetation stands. *J. Geophys. Res.,* **97,** 2697–2715.

Kuchler, A. W., 1988: Natural vegetation. *Goode's World Atlas,* E. B. Espenshade Jr., Ed., 17th ed. Rand McNally, 16–17.

Loveland, T. R., J. W. Merchant, D. O. Ohlen, and J. F. Brown, 1991: Development of a land-cover characteristics database for the conterminous U.S. *Photogramm. Eng. Remote Sens.,* **57,** 1453–1463.

Martner, B. E., 1986: *Wyoming Climate Atlas.* University of Nebraska Press, 432 pp.

Mathews, E., 1983: Global vegetation and land use: New high-resolution data bases for climate studies. *J. Climate Appl. Meteor.,* **22,** 474–487.

Meeson, B. W., F. E. Corprew, J. M. P. McManus, D. M. Myers, J. W. Closs, K.-J. Sun, D. J. Sunday, and P. J. Sellers, 1995: ISLSCP Initiative I—Global Data Sets for Land–Atmosphere Models, 1987–1988. Vols. 1–5. NASA.

Olson, J. S., J. A. Watts, and L. J. Allison, 1983: Carbon in live vegetation of major world ecosystems. DOE/NBB Rep. TR004, 152 pp. [Available from National Technical Information Service, 5285 Port Royal Rd., Springfield, VA 22161.]

Pielke, R. A., G. A. Dalu, J. S. Snook, T. J. Lee, and T. G. F. Kittel, 1991: Nonlinear influence of mesoscale land use on weather and climate. *J. Climate,* **4,** 1053–1069.

Pitman, A. J., 1991: Sensitivity of the land surface to sub-grid scale processes: Implications for climate simulations. *Vegetatio,* **91,** 121–134.

——, Z.-L. Yang, and A. Henderson-Sellers, 1993: Sub-grid scale precipitation in AGCMs: Re-assessing the land surface sensitivity using a single column model. *Climate Dyn.,* **9,** 33–41.

Reed, B. C., J. F. Brown, D. VanderZee, T. R. Loveland, J. W. Merchant, and D. O. Ohlen, 1994: Measuring phenological variability from satellite imagery. *J. Veg. Sci.,* **5,** 703–714.

Running, S. W., T. R. Loveland, L. L. Pierce, R. R. Nemani, and E. R. Hunt, 1995: A remote sensing based vegetation classification logic for global land cover analysis. *Remote Sens. Environ.,* **51,** 39–48.

Saxena, K. G., A. K. Tiwari, M. C. Porwal, and A. R. R. Menon, 1992: Vegetation maps, mapping needs and scope of digital processing of landsat thematic mapper data in tropical region of south-west India. *Int. J. Remote Sens.,* **13,** 2017–2037.

Scott, J. M., and Coauthors, 1993: Gap analysis: A geographic approach to protection of biological diversity. *Wildlife Monogr.,* No. 123, Wildlife Society, 1–41.

Sellers, P. J., Y. Mintz, Y. C. Sud, and A. Dalcher, 1986: A Simple Biosphere Model (SiB) for use within general circulation models. *J. Atmos. Sci.,* **43,** 505–531.

——, J. A. Berry, G. J. Collatz, C. B. Field, and F. G. Hall, 1992: Canopy reflectance, photosynthesis, and transpiration. III: A

reanalysis using improved leaf models and a new canopy integration scheme. *Remote Sens. Environ.,* **42,** 187–216.

——, and Coauthors, 1995: Remote sensing of the land surface for studies of global change: Models-algorithms-experiments. *Remote Sens. Environ.,* **51,** 3–26.

Seth, A., F. Giorgi, and R. E. Dickinson, 1994: Simulating fluxes from heterogeneous land surfaces: Explicit subgrid method employing the Biosphere–Atmosphere Transfer Scheme (BATS). *J. Geophys. Res.,* **99,** 18 651–18 668.

Strahler, A., A. Moody, E. Lambin, and MODIS Land Team Principal Investigators, 1994: MODIS Land Cover Product: Algorithm Theoretical Basis Document Version 3.1. [Available on-line from http://eospso.gsfc.nasa.gov.]

Townshend, J. R. G., and C. O. Justice, 1988: Selecting the spatial resolution of satellite sensors required for global monitoring of land transformations. *Int. J. Remote Sens.,* **9,** 187–236.

——, ——, and V. Kalb, 1987: Characterization and classification of South American land cover types. *Int. J. Remote Sens.,* **8,** 1189–1207.

——, ——, W. Li, C. Gurney, and J. McManus, 1991: Global land cover classification by remote sensing: Present capabilities and future possibilities. *Remote Sens. Environ.,* **35,** 243–255.

——, ——, D. Skole, J.-P. Malingreau, J. Cihlar, P. Teillet, F. Sadowski, and S. Ruttenberg, 1994: The 1 km resolution global data set: Needs of the International Geosphere Biosphere Programme. *Int. J. Remote Sens.,* **15,** 3417–3441.

Tucker, C. J., J. R. G. Townshend, and T. E. Goff, 1985: African land-cover classification using satellite data. *Science,* **227,** 369–375.

Verseghy, D. L., N. A. McFarlane, and M. Lazare, 1993: CLASS—A Canadian land surface scheme for GCMs. II: Vegetation model and coupled runs. *Int. J. Climatol.,* **13,** 347–370.

Weiser, R. L., G. Asrar, G. P. Miller, and E. T. Kanemasu, 1986: Assessing grassland biophysical parameters from spectral measurements. *Remote Sens. Environ.,* **20,** 141–152.

Wilson, M. F., and A. Henderson-Sellers, 1985: A global archive of land cover and soil data for use in general circulation climate models. *J. Climatol.,* **5,** 119–143.